IEEE Access
Multidisciplinary | Rapid Review | Open Access Journal

Received 5 January 2025, accepted 10 February 2025, date of publication 14 February 2025, date of current version 24 February 2025.

Digital Object Identifier 10.1109/ACCESS.2025.3542080

RESEARCH ARTICLE

A Novel Reconfigurable Closed-Chain Leg Mechanism Based on Phase Difference Adjustment for Multiple Walking Motion of Quadruped Robot

HYEONBEOM SHIN[1], JIHO PARK[1], HOSU LEE[2], AND JUNGWON YOON[1], (Member, IEEE)

[1]Department of AI Convergence, Gwangju Institute of Science and Technology, Gwangju 61005, Republic of Korea
[2]Department of Control and Robot Engineering, School of Aerospace Engineering, Gyeongsang National University, Jinju-si, Gyeongsangnam-do 52828, Republic of Korea

Corresponding author: Jungwon Yoon (jyoon@gist.ac.kr)

This work was supported by Culture, Sports and Tourism R&D Program through the Korea Creative Content Agency grant funded by the Ministry of Culture, Sports and Tourism in 2023 (Project Name : Development of personalized exhibition viewing concierge service technology for the visually impaired, Project Number: RS-2023-00303777, Contribution Rate: 100%).

ABSTRACT The utilization of single degree-of-freedom (DOF) closed-chain mechanisms as leg mechanisms of quadruped robots has been studied because of its advantages, such as a lightweight structure and simplified control resulting from the decreased number of actuators needed for operation. Furthermore, to improve the scalability of these approaches, researchers have investigated the use of reconfigurable structures. Nevertheless, the traditional method that relies on adjusting the length of links presents a substantial challenge in achieving precise production of various trajectories while maintaining the centroid positions of those trajectories. We propose a novel reconfigurable structure that utilizes the phase difference between the crank gears to generate desired trajectories accurately. The proposed mechanism guarantees that the centroid positions of multiple trajectories remain confined inside the specified border. Comparison with conventional reconfigurable mechanisms demonstrates the ability of the proposed mechanism to achieve high trajectory accuracy over multiple trajectories, even in environments with limited centroid position changes. Additionally, a gait stability analysis of a quadruped robot with the proposed leg mechanism in a simulation environment was conducted to verify its suitability.

INDEX TERMS Quadruped robot, leg mechanism, reconfigurable mechanism, path synthesis, gait stability.

I. INTRODUCTION

Wheeled robots are commonly employed in several applications, including transportation and exploration, because of their inherent stability and relatively uncomplicated control systems. Nevertheless, due to the limited accessibility of traditional wheeled vehicles to around half of the Earth's terrestrial surface, other robotic systems are required to carry out missions in regions with complex topography efficiently [1], [2], [3], [4]. Legged robots exhibit discontinuous ground contact during locomotion and can adjust their center of mass in response to the contact position, enabling them to traverse uneven surfaces [5], [6], [7]. Quadruped robots are the subject of ongoing research due to their enhanced walking stability and movement capabilities compared to bipedal robots.

The leg mechanisms utilized in quadruped robots can be classified into open and closed-chain mechanisms based on the kinematic chain. Open-chain mechanisms provide the advantageous capability of generating unconstrained walking trajectories. However, a leg mechanism based on an open-chain requires several actuators with substantial torque, leading to increased cost of energy and control complexity [8], [9], [10]. In contrast, closed-chain mechanisms exhibit a higher payload capacity due to their

The associate editor coordinating the review of this manuscript and approving it for publication was Yangmin Li.

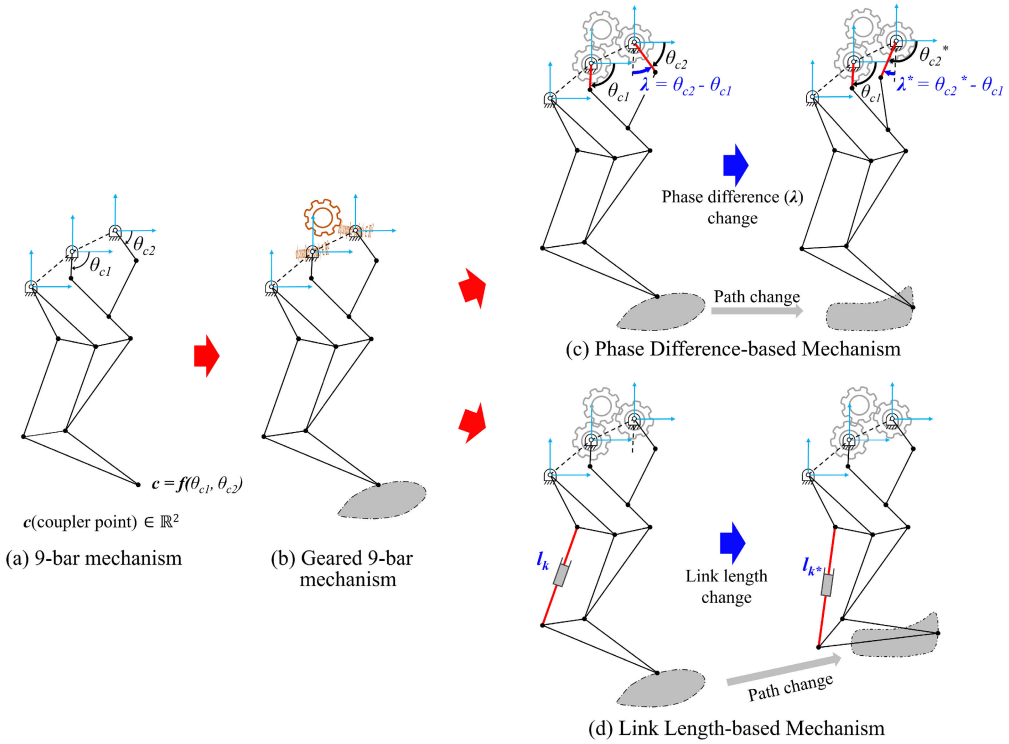

FIGURE 1. Modification process of 9-bar mechanism (a) 9-bar mechanism (b) Geared 9-bar mechanism (c) PDM; Phase Difference-based Mechanism (d) LLM; Link Length-based Mechanism.

inherent structural rigidity, which provides advantages in terms of energy efficiency [11]. In particular, single DOF closed-chain-based leg mechanisms provide advantages in simplification of the system control by utilizing a reduced number of actuators compared to the multi-DOF mechanisms [12]. However, quadruped robots based on single DOF closed-chain mechanisms have low adaptability to change in terrain environments due to their low degree of freedom. Researchers are focused on designing a reconfigurable structure that allows single DOF closed-chain-based leg mechanisms to generate multiple walking trajectories for expanding the flexibility of the gait motion [13].

Several studies focused on enhancing the trajectory flexibility of single DOF closed-chain-based mechanisms by applying reconfigurable link structures to generate multiple trajectories. To apply the Jansen mechanism and the Klann mechanism to a multi-pedal walking robot, Shunsuke et al. and Tan Phuc et al. conducted a study to generate multiple trajectories by changing the link length of the mechanism [14], [15]. Haghjoo et al. used the Jansen mechanism to produce a lower extremity rehabilitation robot with two reconfigurable mechanism links [16]. Based on a variable topology structure, Wu and Yao, Wei et al. applied a reconfigurable single DOF mechanism with one tunable parameter to develop a closed-chain multi-pedal walking robot that generates two different walking trajectories for walking on flat ground and overcoming obstacles [17], [18].

However, these conventional reconfigurable link length-based mechanisms (LLMs) require the attachment of an extra structure to the leg link to adjust the link length, resulting in an augmented payload for the actuator [17]. In addition, LLM leadsÂ to variations in the overall configuration of the leg mechanism due to changes in its link length, hence being able to restrict the range of applications for leg mechanisms.

Therefore, a method is required to reconfigure the shape of the trajectory without any change in the link lengths. However, as far as we know, there is no study of a mechanism that treated components other than link length in a planar mechanism as reconfigurable parameters. Thus, we propose a novel reconfigurable mechanism that utilizes the phase difference between the crank gears, called a Phase Difference-based Mechanism (PDM).

As shown in Figure 1(a), the basic 9-bar mechanism is a 2-DOF structure according to Grübler's criteria, so that the end effector of the mechanism can move two-dimensional coordinates freely. The mechanism can be constrained to a single DOF geared 9-bar mechanism by connecting the two crankshafts through gears as shown in Figure 1(b) [19]. This arrangement allows the gears to rotate while maintaining a constant rotational phase difference. By reconfiguring the phase difference (λ) of the two gears of this geared mechanism as shown in Figure 1(c), multiple trajectories can be generated, and thus, the phase difference can be used as a reconfigurable parameter. The proposal is based on the following hypothesis:

1) When the phase difference between the crank gears is reconfigurable while the link length remains constant, the impact on the variance of the centroid positions

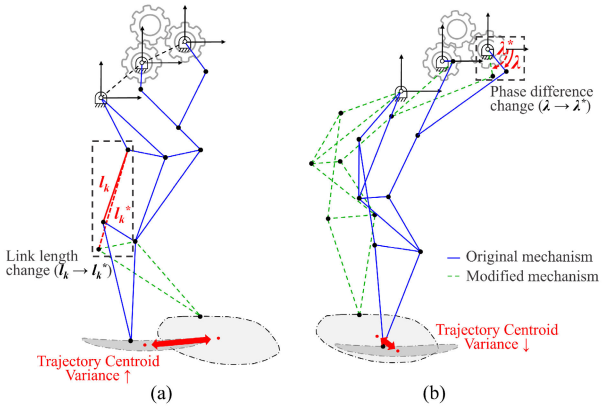

FIGURE 2. Comparison of the trajectory centroid variance between (a) LLM and (b) PDM.

between multiple trajectories is minimized as shown in Figure 2.

2) Therefore, if this mechanism is used as a leg structure for a quadruped robot, gait stability can be secured even when the gait trajectory changes.

Consequently, this study proposes a reconfigurable closed-chain leg mechanism that intends to expand the gait flexibility of closed-chain-based leg mechanisms by enabling precise multi-trajectory generation while maintaining the centroid positions of trajectories.

To evaluate the trajectory tracking performance of mechanisms, path synthesis is conducted for three gait trajectories within the limited centroid variance of the multiple trajectories, and the resulting trajectory accuracy is compared to that of the leg mechanism based on LLM. Three gait trajectories with the walk, trot, and gallop of a border collie, which have the same trajectory centroid position, are chosen as the desired trajectories [20]. Furthermore, to verify the applicability of the proposed mechanism, the walking stability of PDM is validated by simulating three distinct gait modes (walk, trot, gallop) of a quadruped robot utilizing the PDM via Adams™, a commercial dynamic analysis software by MSC Software. The stability analysis assesses not only the PDM but also quadruped robots using LLM, and a comparative analysis between the two types of robots is included.

Our contributions to this study are as follows:

1) We propose a novel single DOF closed-chain mechanism multi-trajectory generation method that uses the phase difference of crank gears as a reconfigurable structure.
2) We verify that the proposed mechanism can synthesize multiple trajectories more precisely than the conventional link length-based reconfiguration method within a limited centroid variance of the multiple trajectories.
3) Through dynamic simulation of a quadruped robot based on a synthesized result of the proposed leg mechanism, we verify that the PDM ensures higher gait stability than the LLM while changing gait mode.

The proposed phase difference-based reconfigurable mechanism design and calculation of the forward kinematics are described in Chapter 2. The path synthesis method for the design process of the proposed mechanism inspired by the optimal tracking control and two-stage path synthesis algorithm of the shadow robot is described in Chapter 3. A comparison between the path synthesis result of the proposed leg mechanism and the conventional leg mechanism is introduced in Chapter 4. The experimental setup of dynamic simulation and results of the locomotion simulation of the quadruped robot based on the proposed and conventional mechanism are described in Chapter 5.

II. PHASE DIFFERENCE-BASED RECONFIGURABLE GEARED 9-BAR MECHANISM

A. PARAMETERIZATION

As shown in Figure 3, the 9-bar mechanism consists of 9 links, 11 revolute joints, and 3 pivots. l_2 and l_5 are one link (l_{25}) but are treated as two different parameters to consider the position of the revolute joint of P_2. l_a and l_b represent the distance between pivots. θ_a and θ_b represent the angles of l_a and l_b with respect to the world coordinate system respectively. Figure 3(a) shows the configuration of the whole mechanism, and the parameterization of the 9-bar mechanism is shown in Figure 3(b-g). The design vector obtained through the parameterization of the 9-bar mechanism is as follows:

$$x_{9-bar\ mechanism} = [l_1; l_2; l_3; l_4; l_5; l_6; l_7; l_8; l_9; l_{10}; l_{11}; l_{12}; l_{13}; l_{14}; l_{15}; l_a; l_b; \theta_a; \theta_b]$$

To constrain the mechanism to 1-DOF, we modified the 9-bar mechanism to a geared 9-bar mechanism that constrains the two crankshafts l_1 *and* l_4 through a gear structure. The phase difference between the two crankshafts is defined as:

$$\lambda = \theta_4 - \theta_1$$

where θ_1 and θ_4 represent the angles of crank l_1 and l_4 respectively with respect to the world coordinate. Therefore, the design vector $x_{geared\ 9-bar\ mechanism}$ of the geared 9-bar mechanism is as follows:

$$x_{geared\ 9-bar\ mechanism} = [l_1; l_2; l_3; l_4; l_5; l_6; l_7; l_8; l_9; l_{10}; l_{11}; l_{12}; l_{13}; l_{14}; l_{15}; l_a; l_b; \theta_a; \theta_b; \lambda]$$

Because the rotation angle of l_4 changes concerning the rotation angle of l_1, the shape of the trajectory generated by the mechanism changes. In other words, multiple trajectories can be generated by changing the parameter λ, which represents the phase difference between the crank gears. Figure 1(c) and Figure 2(b) shows that the shape of the trajectory changes as λ takes multiple values of λ. Thus, the design vector x_{PDM} of PDM is as follows:

$$x_{PDM} = [l_1; l_2; l_3; l_4; l_5; l_6; l_7; l_8; l_9; l_{10}; l_{11}; l_{12}; l_{13}; l_{14}; l_{15}; l_a; l_b; \theta_a; \theta_b, \lambda_t]$$

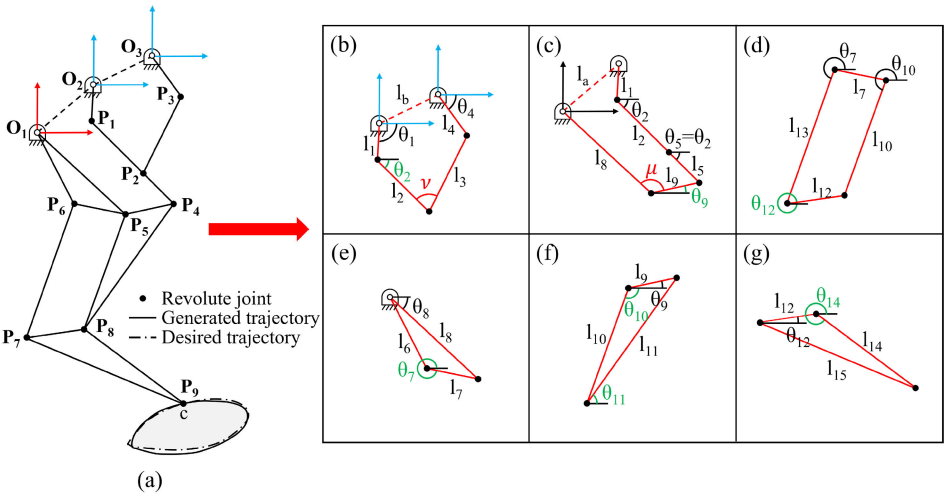

FIGURE 3. Parameterization figure of 9-bar mechanism (a) configuration of whole mechanism (b) five bar part 1 (c) five bar part 2 (d) 4-bar part (e) triangle part 1 (f) triangle part 2 (g) triangle part 3.

where $\lambda_t = [\lambda_1; \lambda_2; \ldots; \lambda_i]$, and λ_i represents the value of the crank link phase difference corresponding with the specific trajectory.

B. FORWARD KINEMATICS

The 9-bar mechanism consists of two 5-bar parts $[O_2, O_3, P_3, P_2, P_1]$, $[O_1, O_2, P_1, P_4, P_5]$, one 4-bar part $[P_5, P_6, P_7, P_8]$, and the triangle parts of $[O_1, P_5, P_6]$, $[P_4, P_5, P_8]$, and $[P_7, P_8, P_9]$ respectively as shown in Figure 3(b-g). The forward kinematics of the 9-bar mechanism are obtained by calculating each part that makes up the mechanism in order.

1) From 5-bar part 1, 2 $\rightarrow$ P_4, P_5 is calculated
2) From triangle part 1, 2 $\rightarrow$ P_6, P_8 is calculated
3) From 4-bar part $\rightarrow$ P_7 is calculated
4) From triangle part 3 $\rightarrow$ P_9 is calculated

As the crank rotates while maintaining a constant phase difference by the geared mechanism, the trajectory generated by P_9 is the coupler point. Coupler point c is expressed by a nonlinear function f for the design vector x and the rotation angle θ_1 of crank link l_1.

$$c = f(x,\ \theta_1)$$

The coordinate c_L of the coupler point c with respect to O_1 in Figure 3(a) is expressed as follows:

$$c_L = \begin{bmatrix} l_1\cos\theta_1 + l_{25}\cos\theta_2 + l_{11}\cos\theta_{11} + l_{14}\cos\theta_{14} \\ l_1\sin\theta_1 + l_{25}\sin\theta_2 + l_{11}\sin\theta_{11} + l_{14}\sin\theta_{14} \end{bmatrix} \quad (1)$$

When O_1 is fixed as the origin of world coordinates, $c = c_L$.

1) 5-BAR PART

To calculate c_L, in addition to θ_2, θ_{11}, and θ_{14} represented in Equation (1), θ_7, θ_9, θ_{10}, and θ_{12} are required to be obtained. θ_2 and θ_9 which are the angles of the 5-bar parts in Figure 3(b, c) can be obtained by following equations.

$$\theta_i = 2\arctan\left(\frac{-B_i + H_i}{I_i}\right), \quad i = 2, 9$$

where:

$$\begin{bmatrix} A_2 \\ A_9 \end{bmatrix} = \begin{bmatrix} 2l_1l_2\cos\theta_1 - 2l_bl_2\cos\theta_b - 2l_2l_4\cos\theta_4 \\ -2l_{25}l_9\cos\theta_2 - 2l_1l_9\cos\theta_1 - 2l_al_9\cos\theta_a \end{bmatrix}$$
$$\begin{bmatrix} B_2 \\ B_9 \end{bmatrix} = \begin{bmatrix} 2l_1l_2\sin\theta_1 - 2l_bl_2\sin\theta_b - 2l_2l_4\sin\theta_4 \\ -2l_{25}l_9\sin\theta_2 - 2l_1l_9\sin\theta_1 - 2l_al_9\sin\theta_a \end{bmatrix}$$
$$\begin{bmatrix} C_2 \\ C_9 \end{bmatrix} = \begin{bmatrix} -2l_1l_b(\cos\theta_1\cos\theta_b + \sin\theta_1\sin\theta_b) \\ 2l_1l_{25}(\cos\theta_1\cos\theta_2 + \sin\theta_1\sin\theta_2) \end{bmatrix}$$
$$\begin{bmatrix} D_2 \\ D_9 \end{bmatrix} = \begin{bmatrix} -2l_1l_4(\cos\theta_1\cos\theta_4 + \sin\theta_1\sin\theta_4) \\ 2l_1l_a(\cos\theta_1\cos\theta_a + \sin\theta_1\sin\theta_a) \end{bmatrix}$$
$$\begin{bmatrix} F_2 \\ F_9 \end{bmatrix} = \begin{bmatrix} l_b^2 + l_4^2 + l_2^2 + l_1^2 - l_3^2 \\ l_1^2 + l_{25}^2 + l_9^2 + l_a^2 - l_8^2 \end{bmatrix}$$
$$G_i = C_i + D_i + E_i + F_i$$
$$H_i = -\sqrt{A_i^2 + B_i^2 - G_i^2}$$
$$I_i = G_i - A_i$$

2) 4-BAR PART & TRIANGLE PART

The angle corresponding to the 4-bar is θ_{12}, and the angle corresponding to the triangle parts is θ_7, θ_{10}, θ_{11}, and θ_{14}. 4-bar part is shown in Figure 3(d), and triangle parts are shown in Figure 3(e-g).

$$\theta_i = 2\arctan\left(\frac{-B_i + H_i}{I_i}\right), \quad i = 7, 10, 11, 12, 14$$

where:

$$\begin{bmatrix} A_7 \\ A_{10} \\ A_{11} \\ A_{12} \\ A_{14} \end{bmatrix} = \begin{bmatrix} -2l_7l_8\cos\theta_8 \\ -2l_9l_{10}\cos\theta_9 \\ -2l_9l_{11}\cos\theta_9 \\ -2l_7l_{12}\cos\theta_9 \\ -2l_{10}l_{12}\cos\theta_{10} \end{bmatrix}$$

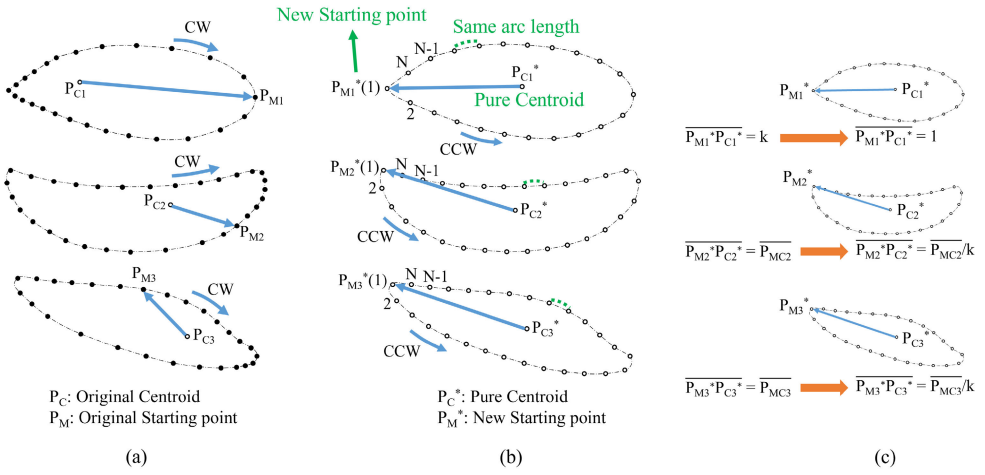

FIGURE 4. Standardization & normalization process (a) original trajectory (b) standardized trajectory and pure centroid (c) standardized and normalized trajectory.

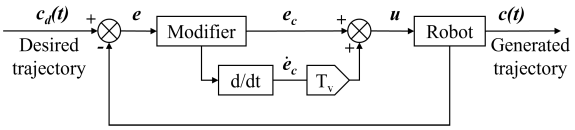

FIGURE 5. PD controller based on the contour error of the shadow robot.

$$\begin{bmatrix} B_7 \\ B_{10} \\ B_{11} \\ B_{12} \\ B_{14} \end{bmatrix} = \begin{bmatrix} -2l_7l_8\sin\theta_8 \\ -2l_9l_{10}\sin\theta_9 \\ -2l_9l_{11}\sin\theta_9 \\ -2l_7l_{12}\sin\theta_9 \\ -2l_{10}l_{12}\sin\theta_{10} \end{bmatrix}$$

$$\begin{bmatrix} C_7 \\ C_{10} \\ C_{11} \\ C_{12} \\ C_{14} \end{bmatrix} = \begin{bmatrix} l_7^2 + l_8^2 - l_6^2 \\ l_9^2 + l_{10}^2 - l_{11}^2 \\ l_9^2 + l_{11}^2 - l_{12}^2 \\ \alpha \\ l_{13}^2 + l_{14}^2 - l_{15}^2 \end{bmatrix}$$

$$\alpha = 2l_7l_{10}\cos\theta_7\cos\theta_{10} + 2l_7l_{10}\sin\theta_7\sin\theta_{10} + l_7^2 + l_{10}^2 + l_{12}^2 - l_{13}^2$$

$$G_i = C_i + D_i + E_i + F_i$$

$$H_i = -\sqrt{A_i^2 + B_i^2 - G_i^2}$$

$$I_i = G_i - A_i$$

III. PATH SYNTHESIS METHOD OF THE PDM-BASED GEARED 9-BAR MECHANISM

The temporal synchronization of the trajectories between the four legs in the quadruped robot is an essential factor in ensuring stability. In existing error-based path synthesis approaches, ensuring that the coupler point c of the mechanism accurately follows the desired path and maintains the correct timing throughout the duration presents a significant challenge. The path synthesis method provided in [21] has been modified to enhance the timing accuracy of the trajectory of the proposed PDM-based leg mechanism. Furthermore, to address the issue of local optima resulting from the high dimensionality of the optimization parameter vector, the two-stage trajectory synthesis algorithm was applied [22].

A. OPTIMAL TRAJECTORY TRACKING CONTROL OF SHADOW ROBOT BASED ON CONTOUR ERROR

For the path synthesis process, the objective function used in the optimization is calculated using the contour error between the desired trajectory and the generated trajectory. Contour error e_c, which is explained especially well in the literature regarding the precise tracking of computer numerical control machines, means the error from the point on the desired trajectory to the point closest to the generated trajectory when time is t_i [21], [23].

$$e_c(i) = min\,|c_d(j) - c(i)| \quad for\ j \in \left[i - \frac{\Delta}{2}, i + \frac{\Delta}{2}\right] \tag{2}$$

where $c_d(j)$ is the j^{th} point of the discretely expressed desired trajectory, $c(i)$ is the ith point of the generated trajectory of the shadow robot, and Δ is the arbitrary threshold value for the error comparison area.

For the efficiency of the optimization process, the design vector x of the mechanism is defined as the shadow robot that tracks the trajectory through each actuator located on each design parameter. As shown in Figure 5, feedback control with a PD controller of the control law u for the control of the shadow robot was used where the input is desired points, and the output is generated points.

$$u = e_c + T_v\dot{e}_c$$

where e_c and $\dot{e}_c(i) = e_c(i) - e_c(i-1)$ mean contour error and its derivative, respectively. And T_v is the derivative time constant of the PD control law u [21].

By adding the norm of u at all points, the objective function J is the contour error of the generated trajectory of the shadow robot to the desired trajectory.

$$J = \sum_{i=1}^{N} \omega(i)\,\|u(i)\| = \sum_{i=1}^{N} \omega(i)\,\|e_c(i) + T_v\dot{e}_c(i)\| \tag{3}$$

where N is the number of points that make up the desired trajectory and the generated trajectory, and $\omega(i)$ means the weight for each point in the trajectory.

B. TWO-STAGE TRAJECTORY SYNTHESIS ALGORITHM

The two-stage trajectory synthesis algorithm proposed in [22] minimizes the calculation efforts by reducing the influence of the scale and position of the trajectory and the number of optimization parameters.

The first stage is about pure shape optimization, which includes standardization and normalization of the trajectory. Standardization is the process of rearranging the points of the trajectory according to specific standards to minimize the influence of the arrangement of the points within the trajectory, and normalization is the process of minimizing the influence of the trajectory size by fixing the distance between the starting point and the pure centroid to 1. The standardization and normalization of the trajectory process, according to Figure 4, are organized as follows:

1) Rearrange the points so that the arc lengths of the neighboring points of the trajectory are constant. Assume that all masses are fixed.
2) Calculate the position of the centroid of the rearranged points. It is called pure centroid $P_C{}^*$.

$$P_C{}^* = \frac{1}{N}\sum_{i=1}^{N} P(i)$$

where $P(i)$ is i^{th} rearranged point and N is the number of points.

3) Find the point at the furthest distance from the $P_C{}^*$ and then mark the $P_M{}^*$ as the starting point of the trajectory.
4) Arrange the points counter-clockwise regardless of the rotation direction of the crank.
5) Set the distance $\overline{P_M^* P_C^*}$, which is the connection line segment of the pure centroid $P_C{}^*$ and starting point $P_M{}^*$, equal to 1.

After the first stage, the trajectory produced becomes a pure shape, and the objective function is calculated by comparing the pure shape with the desired trajectory that has undergone the standardization and normalization process.

The optimized trajectory based on the objective function does not match the desired trajectory in the origin scale because the scale and position of the trajectory changed during the standardization and normalization process. Therefore, in the second stage, called the ''matching process,'' the compensation of the scale and position changed from the first stage is needed. After increasing the scale of $\overline{P_M^* P_C^*}$ by l_1, the shape and arrangement of the mechanism can be determined accordingly.

C. PATH SYNTHESIS OF THE PDM

For the path synthesis of the reconfigurable mechanism, the existing path synthesis algorithm must be modified to allow the simultaneous generation of multiple trajectories. Generating an optimum trajectory using this path synthesis algorithm can be divided into the following stages: mechanism normalization, trajectory standardization and normalization, constraints evaluation, objective function computation, and matching.

The coordinates of point O_1 are set as $(0, 0)$. The normalization process removes the scaling factor (l_1) from the design vector. It is accomplished through the normalized or reduced optimization vector $\bar{x}_{PDM}$ in which the link length term is redefined as the ratio $\bar{l}_i = l_i/l_1$ to crank link l_1 as follows:

$$\begin{aligned}\bar{x}_{PDM} = [&\bar{l}_2; \bar{l}_3; \bar{l}_4; \bar{l}_5; \bar{l}_6; \bar{l}_7; \bar{l}_8; \bar{l}_9; \bar{l}_{10}; \bar{l}_{11}; \bar{l}_{12};\\ &\bar{l}_{13}; \bar{l}_{14}; \bar{l}_{15}; \bar{l}_a; \bar{l}_b; \theta_a; \theta_b, \lambda_1; \lambda_2; \lambda_3]\end{aligned} \tag{4}$$

Since the reconfigurable mechanism generates three trajectories simultaneously, three standardization and normalization of trajectory processes are performed. The standardization process is completed by repeating the previously described process for each trajectory. However, there are some things to be careful about during the normalization process. When normalization is performed on all three trajectories, the three $|P_{MC}|$ described above are generated. Therefore, the optimized design vector has not only three crank phase difference values but also three scale values. In this case, the scale changes every time, and all link lengths should be changed according to trajectory changes. Since only one scale term is needed, normalization is performed on the first trajectory, and the remaining two trajectories are reduced by the first trajectory's reduced scale. Hence, assuming the scale of the initial trajectory is denoted by the variable ''k'' and the distances between the centroid and the starting points of the second and third trajectories, before normalization, are represented by the variables $\bar{P}_{MC2}$ and $\bar{P}_{MC3}$ respectively. Then the pure centroid after normalization can be expressed as the distance between points denoted as $\bar{P}_{MC2}/k$, $\bar{P}_{MC2}/k$ as shown in Figure 4(c).

The objective function is based on the contour error of the corresponding desired trajectory, and the generated trajectory has the form of Equation 3, and the objective function for all three trajectories is the form of combining them all as follows:

$$\begin{aligned}J &= \sum_{j=1}^{3}\sum_{i=1}^{N} \omega(j)\omega(i)\,\|u(i,j)\|\\ &= \sum_{j=1}^{3}\sum_{i=1}^{N} \omega(j)\omega(i)\,\|e_c(i,j) + T_v\dot{e}_c(i,j)\|\end{aligned} \tag{5}$$

where $\omega(j)$ is the weight for each trajectory.

Additionally, constraints consist of three mechanism constraints (boundary condition, Grashof criteria, and transmission angle constraint) and one trajectory constraint. The mechanism constraints include boundary conditions for each design parameter to be satisfied to operate normally.

$$x_{k,min} \le x_k \le x_{k,max}\ ;\quad x_k \in \bar{x}_{opt}$$

The 5-bar Grashof criteria are included to ensure that 5-bar part 1 in Figure 3(b) of a geared 9-bar mechanism has

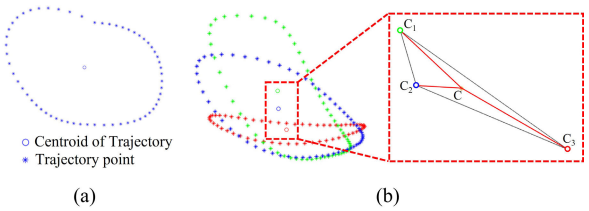

FIGURE 6. Position difference between generated trajectories (a) Centroid of the trajectory (b) Process to calculate position difference between trajectories.

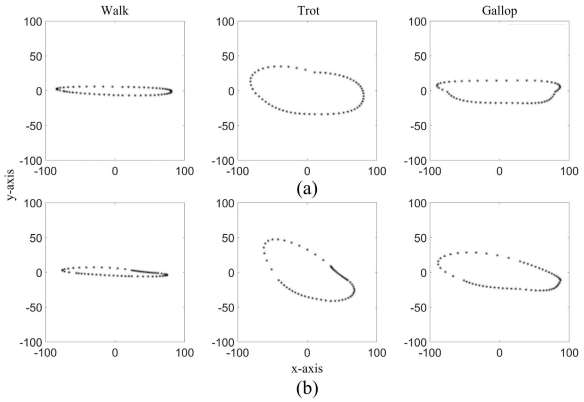

FIGURE 7. The desired trajectory for the synthesis of (a) forward leg (b) hind leg.

two cranks, and 5-bar part 2 in Figure 3(c) has more than one crank [24].

$$min_1(l_1, l_2, l_3, l_4, l_b) + min_2(l_1, l_2, l_3, l_4, l_b) = l_1 + l_4$$

where min_1 and min_2 mean $1st$ and $2nd$ minimum, respectively.

Both 5-bar parts must include transmission angle constraints to ensure no singularities exist.

$$0^\circ < \mu < 180^\circ \ \& \ 0^\circ < \nu < 180^\circ$$

where μ and ν are transmission angles which mean $\mu = \theta_8 - \theta_9 + 180^\circ$ and $\nu = \theta_2 - \theta_3$, respectively as shown in Figure 3(b, c).

Trajectory constraints include constraints that restrict the centroid variance between the multiple trajectories. Changes in the position of multiple trajectory centroids can cause the contact position to shift, resulting in an unstable gait for a quadruped robot. Therefore, to use the PDM to expand the flexibility of gait motion, it is necessary to constrain the variance of the centroid. The constraint to limit the variance of the centroids of trajectories is as follows:

$$\begin{aligned} &Position\ Difference\ (PD) \\ &= \sqrt{\frac{(C - C_1)^2 + (C - C_2)^2 + (C - C_3)^2}{3}} \\ &\leq D \end{aligned} \tag{6}$$

where C_1, C_2, and C_3 represent the pure centroid coordinates of the walk, trot, and gallop trajectories, respectively, and C represents the centroid of the C_1, C_2, and C_3 coordinates as shown in Figure 6. To determine the value of D, optimization is repeated by increasing the value by a constant from 0.1. Since we cannot repeat too many optimizations, the constant is adopted as 0.1. D is set to 0.5 because optimization is not adequately performed when D has a value lower than 0.4.

TABLE 1. Initial value of optimization parameters. PN: Parameter name, UB: Upper bound, LB: Lower bound, F: Forward, H: Hind, IC: Initial condition.

PN		l_1	l_2	l_3	l_4	l_5	l_6
UB	F		12	12	12	12	12
	H		20	20	20	20	20
LB			1	1	1	1	1
IC		1	6.67	5.87	1.8	1.96	4.4
PN		l_7	l_8	l_9	l_{10}	l_{11}	l_{12}
UB	F	12	12	12	12	12	12
	H	20	20	20	20	20	20
LB		1	1	1	1	1	1
IC		4.34	8.34	3.8	5.6	9.24	2.57
PN		l_{13}	l_{14}	l_{15}	l_a	l_b	
UB	F	12	12	12	12	12	
	H	20	20	20	20	20	
LB		1	1	1	1	1	
IC		7.3	5.87	8	1	5	

To apply the defined constraints to the path synthesis of the mechanism, we defined the penalty function P as follows.

$$P = M \times max(g, 0), \quad where\ M = 1000$$

$$g = \begin{cases} 0, & when\ all\ contraints\ are\ satisfied \\ 1, & when\ any\ contraints\ is\ not\ satisfied \end{cases}$$

The final form J_f of the objective function, including penalty function P is as follows:

$$\begin{aligned} J_f &= \sum_{j=1}^{3} \sum_{i=1}^{N} \omega(j)\omega(i) \left\| u(i,j) \right\| \\ &= \sum_{j=1}^{3} \sum_{i=1}^{N} \omega(j)\omega(i) \left\| e_c(i,j) + T_v \dot{e}_c(i,j) \right\| + P \end{aligned}$$

In the optimization of this study, the control loop is terminated only when the initial optimization parameter

$$\bar{x}_{PDM}(0) = \text{argmin}\, J_f$$

is found, and the optimized PDM can be obtained through the subsequent matching process.

IV. COMPARISON OF THE PATH SYNTHESIS RESULT

In this section, problems of the PDM path synthesis are solved. The desired trajectories used in path synthesis are based on the parameterized Bezier curves of the border collie introduced in [20] and shown in Figure 7.

1) The walk, trot, and gallop locomotion trajectories of the border collie's forward legs
2) The walk, trot, and gallop locomotion trajectories of the border collie's hind legs

Table 1 shows the initial parameters, upper boundary, and lower boundary of the optimization parameters in each problem. The forward legs are constrained by the upper

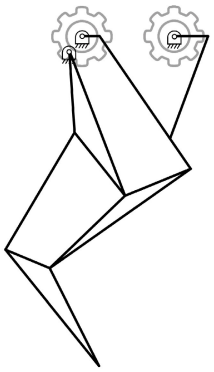

FIGURE 8. Initial configuration of the geared 9-bar leg mechanism.

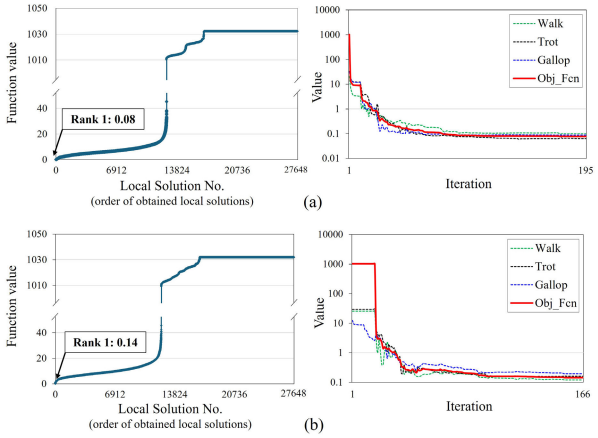

FIGURE 9. The value of the objective function for all local solutions and the response of the contour error and objective function of the rank 1 solution of (a) the forward and (b) the hind leg with PDM.

boundary = 12, and the hind legs are constrained by the upper boundary = 20. However, the initial condition and lower boundary condition are the same in each case. Figure 8 displays the configuration of the mechanism shown through the initial value of the parameter. In this figure, θ_a, θ_b, and three λ is set to 51.57°, 0°, 0°, 0°, and 0°.

The multi-start strategy is adopted to thoroughly search for a global minimum or multiple local minima of the objective function. The initial values of θ_a and θ_b are selected between 0° and 30° with an interval of 10°. The initial values of three λ are selected between 0° and 330° with an interval of 30°. Thus, 27,648 of the initial conditions are explored, and among them, the rank 1 solution that produces the most optimal value is selected as the leg mechanism, as shown in Figure 9. As can be seen, the optimal values of the objective function were 0.08 and 0.14 for the forward and hind legs. Responses of contour error and objective function for the optimal solutions are also shown in Figure 9.

To compare PDM with the conventional reconfigurable mechanism, LLM is synthesized in the same way as the synthesis process of PDM. LLM varies depending on which link length is adopted as a reconfigurable parameter. Among the optimization parameters of the geared 9-bar mechanism, 16 LLMs are synthesized, excluding scale (l_1), orientation (θ_a, θ_b), and crank link phase (λ), and selecting the remaining link length parameters as reconfigurable parameters, respectively. The PDM and LLM synthesis results are shown in Table 2.

TABLE 2. Objective function value (cost) and position difference (PD) of mechanisms with each reconfigurable parameter (RP). F: Forward, H: Hind.

	RP	l_1	l_2	l_3	l_4	l_5	l_6
Cost	F		0.35	0.92	0.1137	0.55	6.36
	H		1.16	0.78	2.77	1.85	0.89
	RP	l_7	l_8	l_9	l_{10}	l_{11}	l_{12}
	F	0.27	1032.23	0.23	0.63	0.21	0.1136
	H	0.40	1032.04	0.23	9.04	0.81	0.20
	RP	l_{13}	l_{14}	l_{15}	l_a	l_b	$\lambda(PDM)$
	F	0.31	1.88	0.64	0.36	0.15	0.08
	H	0.81	2.73	2.82	3.08	0.91	0.14
PD	RP	l_1	l_2	l_3	l_4	l_5	l_6
	F		0.11	0.17	0.02	0.13	0.00
	H		0.25	0.50	0.00	0.21	0.19
	RP	l_7	l_8	l_9	l_{10}	l_{11}	l_{12}
	F	0.16	0.03	0.16	0.01	0.11	0.08
	H	0.17	0.00	0.37	0.00	0.50	0.49
	RP	l_{13}	l_{14}	l_{15}	l_a	l_b	$\lambda(PDM)$
	F	0.23	0.20	0.06	0.14	0.50	0.09
	H	0.22	0.17	0.04	0.39	0.50	0.13

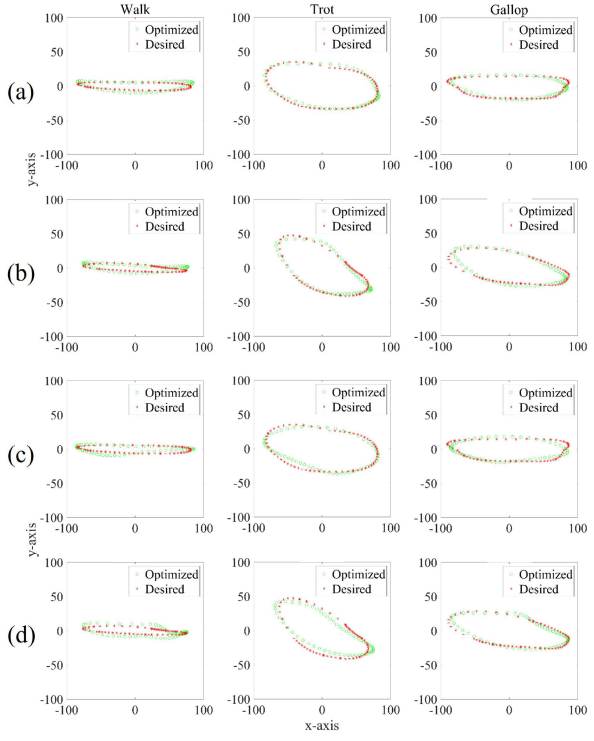

FIGURE 10. Optimized trajectories (green circle) & desired trajectories (red asterisk) of (a) PDM forward leg, (b) PDM hind leg, (c) LLM forward leg based on reconfigurable l_{12}, and (d) LLM hind leg based on reconfigurable l_{12}.

The cost and the position difference (PD) between the centroids of the generated trajectories in Equation (5) are observed as a result of the path synthesis. The RP represents the reconfigurable parameters that a specific mechanism reconfigures to create multiple trajectories.

1) *Forward leg*: According to Table 2, PDM indicates the lowest cost of the path synthesis problem for border collie's

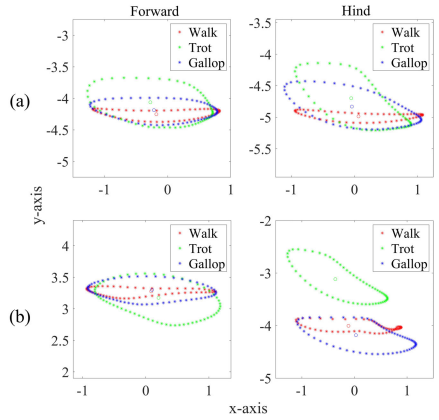

FIGURE 11. Position difference between trajectories of (a) PDM (b) LLM based on reconfigurable l_{12}.

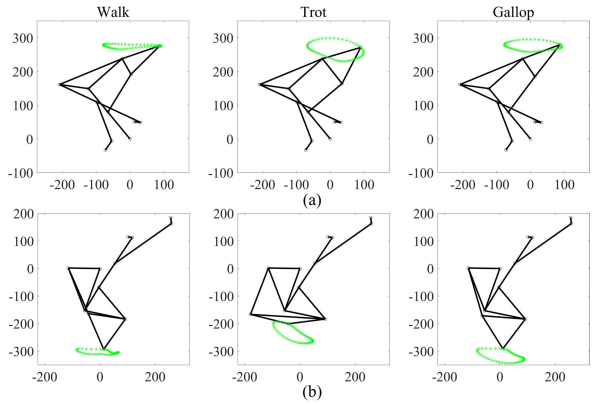

FIGURE 12. Optimized mechanism configuration of LLM-based on reconfigurable l_{12} (a) forward leg (b) hind leg.

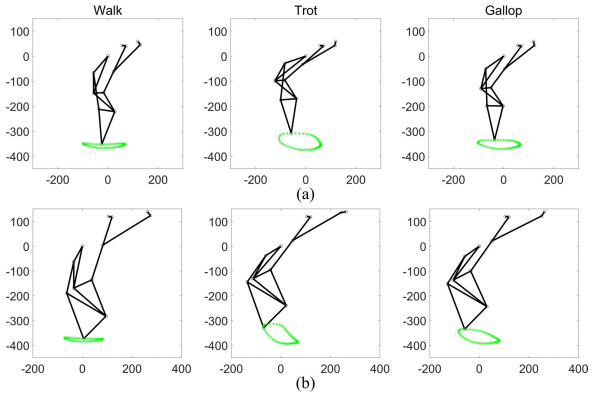

FIGURE 13. Optimized mechanism configuration of PDM (a) forward leg (b) hind leg.

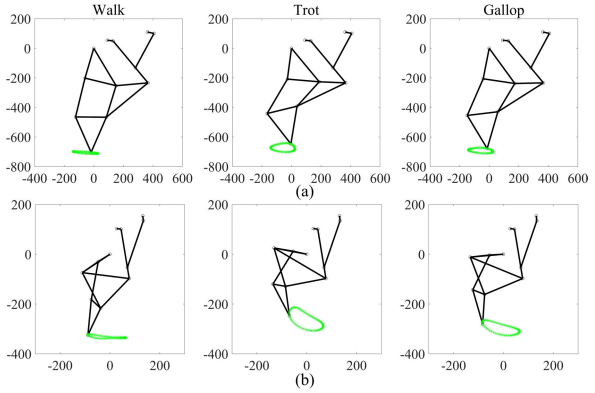

FIGURE 14. Optimized mechanism configuration of LLM based on reconfigurable l_9 (a) forward leg (b) hind leg.

forward leg trajectories, and specifically, the value of cost is 0.08. The second lowest cost of the path synthesis for the forward leg is 0.1136, which is for LLM based on l_{12}. As shown in Figure 10, not only the optimized trajectories of the PDM but also that of LLM based on the l_{12} demonstrate comparable shapes to the desired trajectories. However, the cost of the PDM is 31.70% lower, compared to that of LLM based on l_{12}. Moreover, the cost of the PDM is even 66.11% lower than the third lowest cost, which is for LLM based on l_9. These optimization results show numerically significant differences, although they may seem similar in the figure.

2) *Hind leg*: The result of the path synthesis problem for border collie's hind leg is also represented in Table 2. PDM indicates the lowest cost and specifically has a value of 0.14. The second lowest cost of path synthesis for the hind leg is 0.20, which is of LLM based on l_{12}. The cost of the PDM is 27.96% lower compared to that of LLM based on l_{12}. It is even 36.55% lower than the third lowest cost of LLM based on l_9. As shown in Figure 10, like path synthesis results for the forward leg optimization problem, the optimized trajectories of the LLM based on the l_{12} demonstrate comparable shapes to the desired trajectories. However, it can be indicated that PDM has numerically better results than LLM. Furthermore, when analyzing the centroid variance between trajectories from Figure 11 and Table 2, that of PDM seems low and is numerically low in both optimization problems. On the other hand, that of LLM is low in the forward leg optimization problem, but in the hind leg optimization problem, the trot trajectory deviates from both the walk and gallop trajectories.

The conclusions are as follows: In our two path synthesis problems, PDM indicates the lowest cost in both cases. Thus, it can be concluded that PDM improves the trajectory tracking accuracy more than other LLMs. Furthermore, compared to the LLM, the PDM will exhibit a considerable capacity for maintaining stability when applied to the quadruped robot, with slight variation of the centroid of the trajectories.

V. SIMULATION RESULTS

A. ROBOT DESIGN

Dynamic simulation with Adams™ simulator of the customized quadruped robot model based on the synthesized mechanisms are conducted to verify the applicability of the proposed mechanism as a reconfigurable leg mechanism and to compare it with the LLM. The leg mechanism adopted on the quadruped robot is designed with the forward and hind leg mechanisms of the PDM and LLM synthesized in the previous chapter. LLM based on l_9 is selected as the target for comparison with PDM rather than LLM based on l_{12}. Previously, it was shown that in two-stage optimization, the trajectory scale and position are not arbitrarily set to track the desired trajectory accurately. As a result, the trajectory

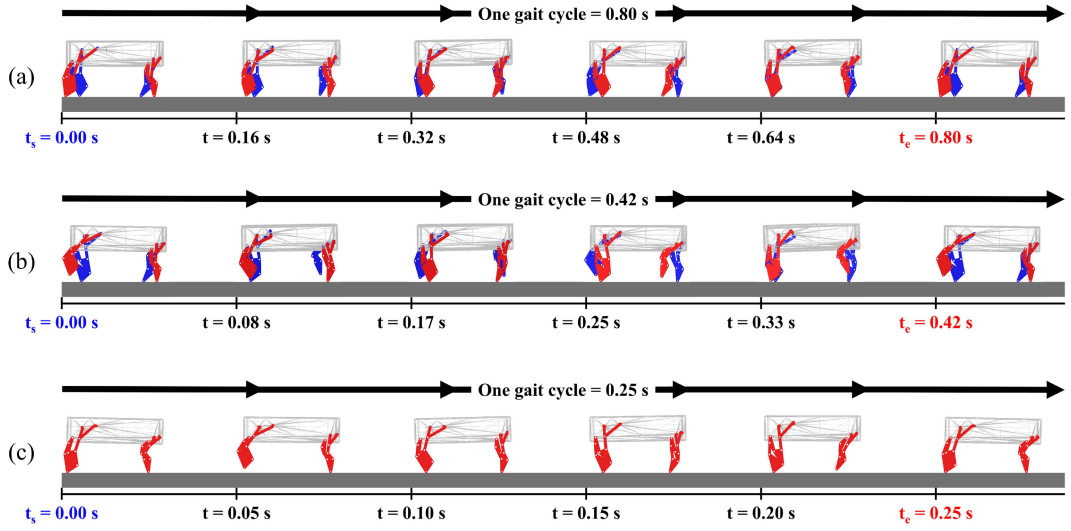

FIGURE 15. Locomotion in gait simulation of PDM-based quadruped robot (a) walk (b) trot (c) gallop.

generated by the LLM based on l_{12} was created in a position that could not allow the quadruped robot to walk. This is shown in Figure 12. Since the top and bottom of the gait trajectory used for optimization are fixed, the mechanism for a quadruped robot to walk must be synthesized by the way that the bottom of the trajectory touches the ground. The forward leg of LLM based on l_{12} shown in Figure 12(a) was synthesized with the end effector facing upward, so the bottom of the trajectory cannot touch the ground.

Therefore, among the LLMs excluding LLM based on l_{12}, LLM based on l_9, which allows trajectory tracking with the highest accuracy, was selected as a comparison target. A visual representation of PDM and LLM based on l_9 can be seen in Figure 13 and Figure 14.

B. SIMULATION ANALYSIS

1) ROBOT STABILITY ANALYSIS

Variation of Center of Mass (CoM) angle is a general indication of the stability of the robot's locomotion [25]. To analyze the stability of locomotion, the stability index q proposed in [26] was used in the analysis of locomotion simulation.

$$q = \sqrt{\frac{\sum_{i=1}^{n_t}\left[(R_i-\bar{R})^2+(P_i-\bar{P})^2+(Y_i-\bar{Y})^2\right]}{n_t}}$$

where R_i, P_i, and Y_i represent roll, pitch, and yaw angle of the CoM at the i^{th} step, respectively, $\bar{R}$, $\bar{P}$, and $\bar{Y}$ represent the average angle values of the CoM in roll, pitch, and yaw angles, respectively, and n_t represents the number of simulation timesteps. q is a value that represents the fluctuations in roll, pitch, and yaw. The smaller the value, the more stable the robot's locomotion is.

To analyze the stability of the robot from the straight walking, simulations were conducted for 10 seconds for each of the robot's walk, trot, and gallop walking modes. Each step corresponds to a time interval of 1e-2 seconds. Before the simulation starts, the robot is slightly floating in the air. Then the robot's locomotion was achieved by varying the rotation phase of the crank link (l_4) between each robot leg. The phase difference of the crank link between each robot leg in each locomotion mode is shown in Table 3. Parameter settings in the simulation environment are summarized in Table 4. Specifically, static and dynamic coefficients are friction coefficients, and stiffness and damping are contact conditions. In all simulations applying PDM and LLM, the size of the robot body, excluding the legs, is the same, and the CoM of the entire robot, including the legs, is located at the exact location within the robot body. The range of possible moving speeds the robot can walk, trot, and gallop in the simulation environment is measured. Since the actual speed of the robot is proportional to the rotation speed of the cranks, the rotation speed of the cranks was measured as possible moving speeds of the robot. A quadruped robot with PDM can walk and trot up to 2520°/s while increasing the crank rotation speed by 90°/s. Additionally, it was confirmed that the robot walked normally in the range of 1350°/s to 2520°/s in gallop mode. In the same experiment, a quadruped robot with LLM can walk up to 810°/s and trot up to

TABLE 3. Phase difference of crank between each leg.

Mode	Hind angle - Forward angle (°)	Left angle - Right angle (°)
Walk	180	180
Trot	180	180
Gallop	135	0

TABLE 4. Parameter conditions of the simulation.

Parameter	Gravity (N/kg)	Static coefficient	Dynamic coefficient	Stiffness (N/mm)	Damping (Ns/mm)
Value	9.81	1.0	0.8	1.0E+05	10.0
Parameter	Weight (kg)	Width (mm)	Height (mm)	Length (mm)	
Value	2.45	104	≒160	220	

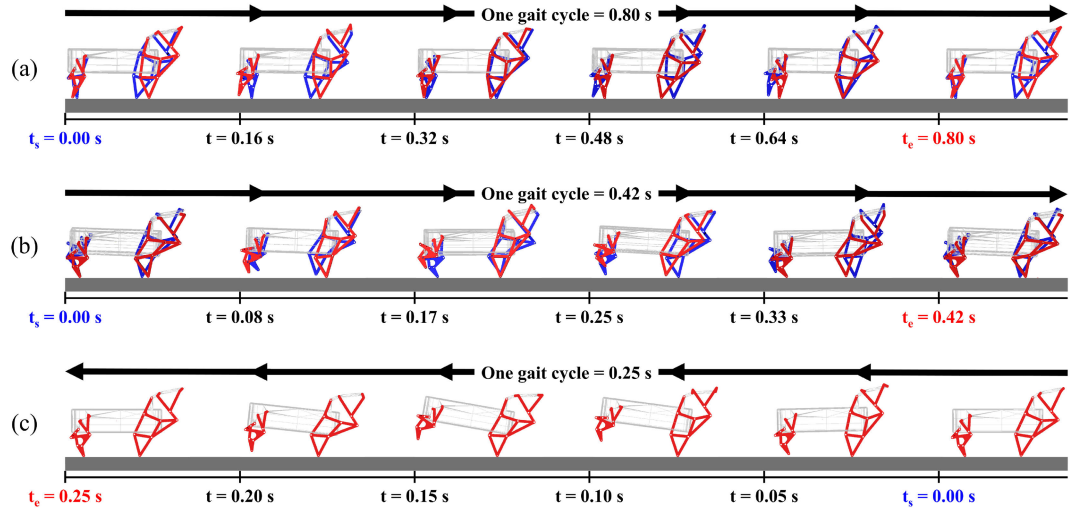

FIGURE 16. Locomotion in gait simulation of LLM-based quadruped robot (a) walk (b) trot (c) gallop.

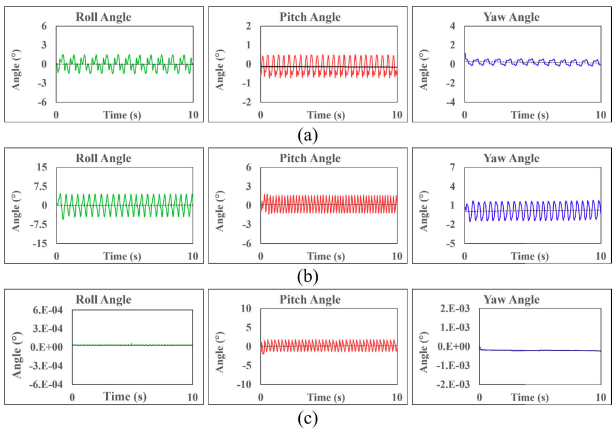

FIGURE 17. Roll, Pitch, and Yaw angle curves of PDM-based quadruped robot (a) walk (b) trot (c) gallop.

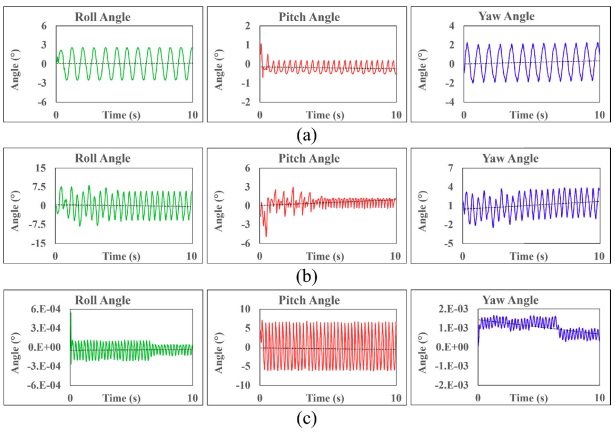

FIGURE 18. Roll, Pitch, and Yaw angle curves of LLM-based quadruped robot (a) walk (b) trot (c) gallop.

1620°/s. However, forward locomotion of the LLM-based quadruped robot was impossible in gallop mode. The moving speed of the robot during stability analysis was derived from the measured range of possible moving speeds. The moving speeds in walk and trot modes are 450°/s and 855°/s, which are the median values of the ranges in which PDM and LLM-based robots can walk simultaneously. Since the LLM-based robot could not walk forward in gallop mode, an arbitrarily set moving speed of 1440°/s was given in gallop mode. The locomotion of the robots in Adams™ simulation is shown in Figures 15 and 16. In Figures 15 and 16, (a), (b), and (c) correspond to distinct modes, while each series of images illustrates one complete gait cycle. Here, $t_s = 0.00$ denotes the initiation of the gait cycle, and t_e represents its termination. The duration of a gait cycle is 0.80 s, 0.42 s, and 0.25 s for walk, trot, and gallop mode. The arrows in the figures indicate the robot's movement direction. Notably, the opposing arrow in Figure16(c) highlights that, in the gallop mode, the LLM-based robot exclusively generated backward locomotion, as opposed to forward locomotion.

TABLE 5. Stability index q of the quadruped robot in locomotion simulation.

	mode	walk	trot	gallop
q	PDM	0.93	3.10	0.97
	LLM	2.23	4.33	-

The locomotion stability analysis for three modes is performed. As a result, the calculated stability parameter q is represented in Table 5. The lower q value of the PDM-based quadruped robot compared to the LLM-based quadruped robot shows that PDM satisfies the trajectory position constraints and ensures gait stability. It means that the stability of the PDM-based robot is improved than that of the LLM-based robot in every walk, trot, and gallop mode. Because of the height of the trajectory, the q values at the trot mode show a high value among the q values. However, it is 28.41% lower than that of the LLM-based quadruped robot. The fact that the proposed quadruped walking robot based on a PDM is capable of various walking motions while maintaining a constant crank speed over 1350°/s ensures low control complexity and high walking flexibility compared

to leg mechanisms based on existing link length adjustment structures and shows the applicability of the proposed PDM as a leg mechanism.

The roll, pitch, and yaw angle curves of robot CoM are confirmed in more detail through Figure 17 and Figure 18. It can be seen that the fluctuation is reduced in the PDM-based robot than in the LLM-based robot except the pitch angle of walk mode. In the walk mode, the pitch angle fluctuation in the LLM-based robot is 0.13° lower than that of the PDM-based robot. However, PDM demonstrates lower values of 0.98° and 1.06° in roll and yaw, respectively, compared to LLM. While the improvements in roll and yaw angles are notable, the degradation in pitch angle within the PDM is relatively negligible, accounting for only approximately 12 to 13% of the roll and yaw enhancements. Consequently, the q value in the walk mode, which implies a three-dimensional stability index, is approximately 2.4 times enhanced than that of LLM as shown in Table 5. It represents the gait stability in the overall mode has been significantly improved than LLM-based robot.

The primary factors that caused PDM's enhanced locomotion capacity are defined by two key aspects: (1) the capacity of PDM to maintain centroid variance over multiple trajectories and (2) its enhanced accuracy in tracking shape and timing of trajectories.

In contrast to the LLM-based reconfigurable mechanism, the proposed leg mechanism based on PDM provides the accurate generation of multiple trajectories while maintaining the leg mechanism's structure with limited centroid position variance, as shown in Table 2. This implies a new opportunity to address the limitation of previous reconfigurable mechanism studies, which are generally capable of generating trajectories that involve changing centroid positions for each trajectory. However, we did not propose a specific structure for adjusting the phase difference in PDM. Through follow-up studies, we need to focus on designing a phase difference adjustment mechanism that integrates a reconfigurable structure with the driving part of the leg mechanism, unlike the LLM-based mechanism, which requires installing an additional device in the middle of the link to adjust the link length. This integration enables the development of a reconfigurable system with a reduced moment of inertia.

VI. CONCLUSION

Ongoing research is being conducted to enhance the flexibility of single DOF closed-chain leg mechanisms in quadruped robots by utilizing reconfigurable structures within a single DOF mechanism. Most research employs a structure that modifies the link length to achieve this objective, potentially augmenting the number of actuators allocated to each segment of the robotic system. These LLM-based mechanisms cause the variance in the centroid positions between multiple trajectories, leading to instability in the locomotion of the quadruped robot.

We propose a novel single-DOF closed-chain mechanism that generates multiple trajectories using the phase difference between crank gears as a reconfigurable parameter. This mechanism accurately generates three distinct trajectories while maintaining the centroid positions between trajectories. By comparing it with the LLM-based mechanism in the path synthesis process, it is verified that the proposed PDM-based mechanism can accurately generate the three distinct trajectories while maintaining the centroid positions, contributing to the locomotion stability of quadruped robots while changing the gait mode. Through dynamic simulation in Adams™, it was verified that PDM has better gait stability than LLM. Additionally, it significantly reduces the control complexity of a quadruped robot by showing that multiple gait motions are possible while maintaining the rotation speed of the crank constant.

Consequently, properties confirmed in this study of the PDM-based leg mechanism allow the creation of a quadruped robot with variable locomotion and significant payload, even while utilizing a simple control method. It is expected that this characteristic expands the flexibility of gait motion of single-DOF quadruped robots and leads to their adaptability in everyday or industrial tasks. For example, creating proper gait trajectories for various terrain conditions will enable locomotion, such as driving across curbs of the roads on everyday tasks and obstacles, such as pipes or profiles in industrial tasks.

Additionally, for the practical implementation of the PDM proposed in this study, we plan future works focused on developing a gear phase transition structures, optimization with the whole body dynamics, and exploration of trajectory shapes for various terrains.

ACKNOWLEDGMENT

(Hyeonbeom Shin and Jiho Park contributed equally to this work.)

REFERENCES

[1] P. Biswal and P. K. Mohanty, "Development of quadruped walking robots: A review," *Ain Shams Eng. J.*, vol. 12, no. 2, pp. 2017–2031, Jun. 2021.

[2] H. Yang, H. Liu, L. Zeng, J. Wu, and Y.-A. Yao, "Design and analysis of a novel octopod platform with spatial 8R reconfigurable trunk," *Mechanism Mach. Theory*, vol. 205, Mar. 2025, Art. no. 105859.

[3] M. F. Silva and J. T. Machado, "A literature review on the optimization of legged robots," *J. Vibrat. Control*, vol. 18, no. 12, pp. 1753–1767, Oct. 2012.

[4] M. S. Maradkar and P. V. Manivannan, "Kinematics and multi-body dynamics of a bio-inspired quadruped robot with nine linked closed chain legs," in *Proc. Int. Conf. Robot., Current Trends Future Challenges (RCTFC)*, Dec. 2016, pp. 1–6.

[5] S. Kajita and B. Espiau, "Legged robot," in *Springer Handbook of Robotics*. Berlin, Germany: Springer, 2008, pp. 361–389.

[6] S. G. Desai, A. R. Annigeri, and A. TimmanaGouda, "Analysis of a new single degree-of-freedom eight link leg mechanism for walking machine," *Mechanism Mach. Theory*, vol. 140, pp. 747–764, Oct. 2019.

[7] M. Geisert, T. Yates, A. Orgen, P. Fernbach, and I. Havoutis, "Contact planning for the ANYmal quadruped robot using an acyclic reachability-based planner," in *Towards Autonomous Robotic Systems*. Cham, Switzerland: Springer, 2019, pp. 275–287.

[8] S.-W. Kim and D.-H. Kim, "Kinematic analysis of a legged walking robot based on four-bar linkage and Jansen mechanism," *J. Korean Inst. Intell. Syst.*, vol. 21, no. 2, pp. 159–164, Apr. 2011.

[9] J. Wu, Y.-A. Yao, Y. Li, S. Wang, and Q. Ruan, "Design and analysis of a sixteen-legged vehicle with reconfigurable close-chain leg mechanisms," *J. Mech. Robot.*, vol. 11, no. 5, Oct. 2019, Art. no. 055001.
[10] K. V. Nasonov, D. V. Ivolga, I. I. Borisov, and S. A. Kolyubin, "Computational design of closed-chain linkages: Hopping robot driven by morphological computation," in *Proc. IEEE Int. Conf. Robot. Autom. (ICRA)*, May 2023, pp. 7419–7425.
[11] J. Wu and Y.-A. Yao, "Design and analysis of a novel multi-legged horse-riding simulation vehicle for equine-assisted therapy," *Proc. Inst. Mech. Eng., C, J. Mech. Eng. Sci.*, vol. 232, no. 16, pp. 2912–2925, Aug. 2018.
[12] Y. Pan and F. Gao, "Position model computational complexity of walking robot with different parallel leg mechanism topology patterns," *Mechanism Mach. Theory*, vol. 107, pp. 324–337, Jan. 2017.
[13] D. Fedorov and L. Birglen, "Design of a self-adaptive robotic leg using a triggered compliant element," *IEEE Robot. Autom. Lett.*, vol. 2, no. 3, pp. 1444–1451, Jul. 2017.
[14] S. Nansai, N. Rojas, M. R. Elara, and R. Sosa, "Exploration of adaptive gait patterns with a reconfigurable linkage mechanism," in *Proc. IEEE/RSJ Int. Conf. Intell. Robots Syst.*, Nov. 2013, pp. 4661–4668.
[15] J. Kulandaidaasan Sheba, M. Elara, E. Martínez-García, and L. Tan-Phuc, "Trajectory generation and stability analysis for reconfigurable klann mechanism based walking robot," *Robotics*, vol. 5, no. 3, p. 13, Jun. 2016.
[16] M. R. Haghjoo, H. Lee, M. R. Afzal, A. Eizad, and J. Yoon, "Mech-Walker: A novel single-DOF linkage device with movable frame for gait rehabilitation," *IEEE/ASME Trans. Mechatronics*, vol. 26, no. 1, pp. 13–23, Feb. 2021.
[17] J. Wu and Y.-A. Yao, "Design and analysis of a novel walking vehicle based on leg mechanism with variable topologies," *Mechanism Mach. Theory*, vol. 128, pp. 663–681, Oct. 2018.
[18] C. Wei, J. Wu, J. Sun, H. Sun, Y.-A. Yao, and Q. Ruan, "Reconfigurable design of a passive locomotion closed-chain multi-legged platform for terrain adaptability," *Mechanism Mach. Theory*, vol. 174, Aug. 2022, Art. no. 104936.
[19] S. Coros, B. Thomaszewski, G. Noris, S. Sueda, M. Forberg, R. W. Sumner, W. Matusik, and B. Bickel, "Computational design of mechanical characters," *ACM Trans. Graph.*, vol. 32, no. 4, pp. 1–12, Jul. 2013.
[20] A. E. M. Schmerbauch, "Implementation and analysis of rich locomotion behavior on the bio-inspired, quadruped robot serval," Ph.D. dissertation, Technische Univ. Ilmenau, 2017.
[21] M. R. Sabaapour and J. Yoon, "A novel method for optimal path synthesis of mechanisms based on tracking control of shadow robot," *Mechanism Mach. Theory*, vol. 131, pp. 218–233, Jan. 2019.
[22] M. R. Haghjoo and J. Yoon, "Two-stage mechanism path synthesis using optimized control of a shadow robot: Case study of the eight-bar Jansen mechanism," *Mechanism Mach. Theory*, vol. 168, Feb. 2022, Art. no. 104569.
[23] H.-R. Chen, M.-Y. Cheng, C.-H. Wu, and K.-H. Su, "Real time parameter based contour error estimation algorithms for free form contour following," *Int. J. Mach. Tools Manuf.*, vol. 102, pp. 1–8, Mar. 2016.
[24] K.-L. Ting, "Five-bar Grashof criteria," *J. Mech., Transmiss., Automat. Des.*, vol. 108, no. 4, pp. 533–537, 1986.
[25] Y. Shi, S. Li, M. Guo, Y. Yang, D. Xia, and X. Luo, "Structural design, simulation and experiment of quadruped robot," *Appl. Sci.*, vol. 11, no. 22, p. 10705, Nov. 2021.
[26] J. Kim, D. X. Ba, H. Yeom, and J. Bae, "Gait optimization of a quadruped robot using evolutionary computation," *J. Bionic Eng.*, vol. 18, no. 2, pp. 306–318, Mar. 2021.

HYEONBEOM SHIN received the B.S. degree in mechanical engineering from the School of Mechanical Engineering, Gwangju Institute of Science and Technology, Gwangju, South Korea, in 2023, where he is currently pursuing the Ph.D. degree with the Department of AI Convergence. He worked as a Teaching Assistant of robotics at Gwangju Institute of Science and Technology, in 2024. His current research interests include mechatronics, quadruped robots, and mechanism synthesis.

JIHO PARK received the B.S. and M.S. degrees from the School of Mechanical Engineering, School of Integrated Technology, Gwangju Institute of Science and Technology, Gwangju, South Korea, in 2021 and 2023, respectively, where he is currently pursuing the Ph.D. degree with the Department of AI Convergence. He has worked as a Teaching Assistant of robotics at Gwangju Institute of Science and Technology, in 2023. His current research interests include mechatronics, medical robots, and mechanism synthesis.

HOSU LEE received the B.S. and M.S. degrees from the School of Mechanical Engineering, Gyeongsang National University (GNU), Jinju, South Korea, in 2014 and 2016, respectively, the Ph.D. degree from GNU, in 2017, and the Ph.D. degree from the Department of Mechatronics, Gwangju Institute of Science and Technology (GIST), Gwangju, South Korea, in 2022. From 2016 to 2017, he was a Researcher at GNU. He was a Teaching Assistant in mechatronics and robotics at GIST, from 2019 to 2021. He was also a Postdoctoral Researcher at Intelligent Medical Robotics Laboratory and Cognition and Intelligence Laboratory, GIST. In 2023, he joined the Department of Control and Robot Engineering, GNU, where he is currently working as an Assistant Professor. His current research interests include rehabilitation robotics, haptic feedback interfaces, cable-driven parallel robots (CDPR), and locomotion interfaces.

JUNGWON YOON (Member, IEEE) received the Ph.D. degree in mechatronics from Gwangju Institute of Science and Technology (GIST), Gwangju, South Korea, in 2005. From 2001 to 2002, he was a Visiting Researcher at Virtual Reality Laboratory, Rutgers University, Piscataway, NJ, USA, and a Visiting Fellow at the Functional and Applied Biomechanics Section, Department of Rehabilitation Medicine, Clinical Center, National Institutes of Health, Bethesda, MD, USA, from 2010 to 2011. He was also a Senior Researcher at Electronics Telecommunication Research Institute (ETRI), Daejeon, South Korea. From 2005 to 2017, he was a Professor at the School of Mechanical and Aerospace Engineering, Gyeongsang National University, Jinju, South Korea. In 2017, he joined the Department of AI Convergence, GIST, where he is currently working as a Professor. Since 2019, he has been working as the Director of Research Center for Nanorobotics in Brain (RCNB), GIST. He is also a Principal Project Director in several large-scale research projects supported by South Korea Governments in the themes of brain stimulation, drug delivery, and hyperthermia using nano robotics. He has authored or co-authored more than 200 peer-reviewed international journals and conference papers. His current research interests include magnetic particle imaging, bio-nano robot control, and rehabilitation robots. He was a Technical Editor of IEEE/ASME TRANSACTIONS ON MECHATRONICS and an Associate Editor of *Frontiers in Robotics and AI*.